

Supporting Information for:

**Concerted Proton-Electron Transfer Oxidation of Phenols and
Hydrocarbons by a High-Valent Nickel Complex**

Katherine J. Fisher, Margalit L. Feuer, Hannah H. M. C. Lant, Brandon Q. Mercado,
Robert H. Crabtree*, and Gary W. Brudvig*

*Department of Chemistry, Yale University,
New Haven, CT 06520, U.S.A.*

Table of Contents:

Experimental Details.....	S2
Synthetic Procedures.....	S4
Supplementary Figures.....	S5
Discussion of Bond Dissociation Enthalpies/Bond Dissociation Free Energies and Solvent Effects.....	S20
Crystallographic Experimental Details	S22
References.....	S29

Experimental Details

General Methods: Reagents were purchased from Sigma-Aldrich or Alfa Aesar and used as received unless otherwise specified. [NO][BF₄] was purified by sublimation under vacuum before use and stored at -25 °C in a glove box after purification. All solvents were purified prior to use by passing over a column of activated alumina and stored over molecular sieves. Experiments were performed under dinitrogen atmosphere in a glove box or using standard Schlenk technique, unless otherwise noted.

pyalkH¹, 2,6-di-tert-butylphenol-d₁,² dihydroanthracene-d₄³ were prepared according to literature procedures.

Instrumentation and Experimental Methods:

¹H NMR: ¹H NMR spectra were recorded on an Agilent DD2 400 MHz spectrometer and ¹H chemical shifts were referenced to residual solvent. The solution magnetic susceptibility was determined using the Evans method in CDCl₃.⁴

UV-Visible Spectroscopy: Absorption spectra were collected using a Cary 50 spectrophotometer.

High Resolution Mass Spectrometry (HR-MS) of Ni(pyalk)₂ (1): The mass spectral data were obtained from a Thermo Scientific (Waltham, MA) LTQ Orbitrap ELITE mass spectrometer. The sample was directly infused into the mass spectrometer via a micro pump. Data were acquired and analyzed with Xcalibur (v2.1). Resolution was set at 120000, and with a mass range (m/z) generally from 150 to 1000. Exact masses were obtained for the entire broadband spectrum.

HR-MS of [Ni(pyalk)₂]⁺ (2): HR-MS was performed with a Thermo Scientific Orbitrap Velos Pro Mass Spectrometer. HR-MS data were recorded in cation mode with a resolution (FWHM) of at least 30,000 at 400 m/z and averaged over at least 100 spectra. The spray needle was held at 3.5 kV with an injection rate of 10 μL/min, source temperature 44 °C, capillary temperature 225 °C and sheath gas flow rate 8 a.u. Instrument parameters were held constant for all MS experiments.

Gas Chromatography-Mass Spectrometry (GC-MS): GC-MS data were taken on an Agilent 6890N/5973 spectrometer.

EPR: EPR spectra were measured on a Bruker EXELSYS E500 spectrometer utilizing a super-high Q resonator and a liquid nitrogen finger dewar at 77 K. Instrument parameters included microwave frequency: 9.374 GHz; microwave power: 0.00206 mW; modulation frequency: 100 kHz; modulation amplitude: 5.00 G; conversion time 5.12 ms; time constant: 1.28 ms. Samples were prepared at 1 mM in a 1:1 CH₂Cl₂/toluene mixture. Simulations were performed using Matlab and the Easyspin package.⁵

X-ray Photoelectron Spectroscopy: The XPS spectra were collected using a monochromatic 1486.7 eV Al K α X-ray source on PHI VersaProbe II X-ray Photoelectron Spectrometer with a 0.47 eV system resolution. The energy scale was calibrated using Cu 2p $_{3/2}$ (932.67 eV) and Au 4f $_{7/2}$ (84.00 eV) peaks on a clean copper plate and a clean gold foil. The samples were prepared by drop casting a solution of **2** in CH $_2$ Cl $_2$ onto a Si wafer. The reported shifts were referenced using the Si 2p peak (99.3 eV) from the Si wafer.

Electrochemical measurements: Electrochemical measurements were performed on a Pine AFCBP1 bipotentiostat using a standard three-electrode configuration. A boron-doped diamond working electrode and a platinum counter-electrode were used. A silver wire was used as a pseudo-reference electrode, and the potential was referenced using a ferrocene internal standard. Spectra were taken in dry MeCN with 0.1 M tetrabutylammonium hexafluorophosphate used as electrolyte.

Kinetics: Reactions were monitored by stopped-flow (except for the reaction of **2** with THF). All stopped flow experiments were performed at room temperature using an On-line Instruments Systems, Inc. (Olis) U.S.A. Stopped-Flow paired with an Olis RSM 1000 Rapid Scanning Spectrophotometer. In a typical experiment, a 2 mM stock solution of Ni $^{3+}$ (pyalk) $_2$ in CH $_2$ Cl $_2$ was prepared under dinitrogen atmosphere in a glove box, along with solutions of phenol or hydrocarbon substrates at various concentrations. Solutions were transferred to gas-tight stopped flow syringes with Luer Lock tips. Before a run, the stopped-flow mixing lines were flushed with dry CH $_2$ Cl $_2$ and then washed with Ni $^{3+}$ (pyalk) $_2$ or substrate. During the run, equal volumes of Ni $^{3+}$ (pyalk) $_2$ and substrate were mixed, and 500-4000 UV-visible spectra were taken over the course of the reaction. Observed rate constants were determined using global analysis fitting with the SPECFIT/32 software.

The reaction of **2** with THF was monitored by UV-visible spectroscopy on an Agilent 845x UV-visible spectrophotometer. In a typical experiment, **2** was added to a sealable quartz cuvette equipped with a septum top in an N $_2$ -filled glove box. The cuvette was sealed and removed from the glovebox. Dry THF was injected into the cuvette by syringe, shaken briefly to dissolve the solid **2**, and then the first UV-visible spectrum was taken. Observed rate constants were determined using a method of initial rates.

pK $_a$ determination of **1:** Titrations to determine the pK $_a$ of **1** were monitored by UV-visible spectroscopy. As **4** appears to be sensitive to excess acid, the pK $_a$ of **1** was determined by the titration of **4** with DBU to generate **1**. The pK $_a$ was determined from a plot of [DBU] vs. [1][DBU-H $^+$]/[4]. Concentrations of **1**, **4**, DBU, and DBU-H $^+$ were determined by mass balance as described in reference 6.⁶ The titration was performed 3 times, and the final pK $_a$ was found by averaging the pK $_a$ values found in each titration.

Synthetic Procedures

Ni(pyalk)₂ (1): 0.60 g (2.5 mmol) NiCl₂•6H₂O was dissolved in 20 mL MeOH and 40 mL MeCN. 0.70 g of pyalkH (5.1 mmol, 2.1 eq) was added and stirred for several minutes, during which time the color of the solution changed from teal to dark blue. This mixture was allowed to stir for an hour, at which time 1.0 mL (10 mmol, 4 eq) of a 0.1 M solution of KOH in MeOH was added, which caused the solution to turn yellow-green. This solution was allowed to stir for an hour. The solution was then taken to dryness by rotary evaporation, and the solid was redissolved in 5 mL CH₂Cl₂. 25 mL MeCN was added to this solution, and the CH₂Cl₂ was removed by rotary evaporation, resulting in the precipitation of a light green solid from the remaining MeCN. Crystals suitable for X-ray diffraction were grown from diffusion of pentanes into a solution of **1**. ¹H NMR (CDCl₃, 400 MHz): δ_H 8.03 (2H, d), 7.63 (2H, t), 7.07 (2H, t), 6.92 (2H, d), 1.54 (12 H, s) ppm. UV-visible λ_{max}, nm (ε M⁻¹ cm⁻¹): 365 (150), 620 (75). Elemental analysis calculated for NiC₁₆H₂₀N₂O₂: C, 58.05; H, 6.09; N, 8.46. Found: C, 57.96; H, 6.14; N, 8.29. Yield: 0.65 g, 78%.

[Ni(pyalk)₂]⁺ (2): To a 20 mL vial equipped with stir bar, 0.40 g (1.2 mmol) Ni(pyalk)₂ was added and dissolved in 10 mL dry CH₂Cl₂. Excess [NO][BF₄] was added. Within seconds, the light green solution turned dark blue. This solution was allowed to stir for 5 minutes. The solution was then filtered in order to remove any unreacted [NO][BF₄]. The resulting solution was then triturated with 50 mL pentanes, resulting in the precipitation of a dark blue solid. The solid was filtered under vacuum and washed with pentanes. UV-visible λ_{max}, nm (ε, M⁻¹ cm⁻¹): 340 (990), 610 (1025). Evans method μ_{eff}: 1.87 μ_B. EPR (9.4 GW, 77K): Yield: 0.36 g, 75%.

[Ni(pyalk)₂(py)₂]⁺ (3): 0.05 g **2** was dissolved in 2 mL CH₂Cl₂. To this solution, 0.5 mL pyridine was added. The solution immediately turned a bright yellow color. Crystals were obtained by vapor diffusion with pentanes at 0 °C. UV-visible λ_{max}, nm (ε, M⁻¹ cm⁻¹): 415 (1100). EPR (9.4 GW, 77 K): g_x = 2.202, g_y = 2.163, g_z = 2.030. Yield: 0.04 g, 70%.

[Ni(pyalkH)₂][2(Bar^F)] (4): In a reaction of **2** with dihydroanthracene (see below), a blue precipitate was identified. This precipitate was collected by vacuum filtration, dissolved in water and excess NaBar^F was added. This resulting product was then extracted into CH₂Cl₂ and triturated with pentanes, resulting in the formation of a blue solid.

[Ni(pyalkH)₂][2(Bar^F)] (4) alternate synthesis: 0.1 g (0.3 mmol) Ni(BF₄)₂•6H₂O was dissolved in 10 mL H₂O. 0.081 g of pyalkH (0.6 mmol, 2.1 eq) was added and stirred for several minutes. This solution was transferred to a separatory funnel, and excess NaBar^F and CH₂Cl₂ were added. The resulting product was extracted into CH₂Cl₂ and washed 3 times with water. The organic layer was dried over MgSO₄ and brought to dryness by rotary evaporation. The resulting solid was redissolved in CH₂Cl₂, filtered, and layered with pentanes, resulting in a light blue powder. ¹H NMR (CDCl₃, 400 MHz): δ_H 8.53 (2H, d), 8.11 (t, 2H), 7.71 (s, 16H), 7.63 (d, 2H), 7.55 (s, 10H), 1.53 (s, 12H). Elemental analysis calculated for NiC₈₈H₅₆B₂F₄₈N₃O₃: C, 48.14; H, 2.57; N, 1.91. Found: C, 47.94; H, 2.56, N, 2.02 Yield: 0.31 g, 46%.

Ni(pyalkH)₂(OAc)₂ (5): 0.10 g (0.56 mmol) NiOAc₂•4H₂O was dissolved in 10 mL MeOH and 20 mL MeCN. 0.170 g of pyalkH (1.25 mmol, 2.2 eq) was added and stirred for several minutes, during which time the color of the solution changed from teal to bright blue. The solution was brought to dryness by rotary evaporation and redissolved in CH₂Cl₂. This solution was layered with pentanes and stored at -20 °C, affording blue crystals after several days. Elemental analysis calculated for NiC₂₀H₂₈N₂O₆: C, 53.25; H, 6.26; N, 6.21. Found: C, 52.34; H, 6.30, N, 5.96. Yield: 0.18 g, 85%.

Reaction of 2 with 9,10 dihydroanthracene: To a 20 mL vial equipped with stir bar in an N₂-filled glove box, 0.01 g (0.024 mmol) **2** was added. **2** was dissolved in 10 mL dry CH₂Cl₂, and to this solution 0.0095 g (2.2 eq) 9,10-dihydroanthracene was added. The solution was stirred for 4 hr, during which time the color changed from dark blue to light green and slightly cloudy. The solution was removed from the glove box and run over a plug of alumina to remove the reduced nickel species. The resulting solution was then brought to dryness by rotary evaporation and redissolved in CDCl₃ for ¹H NMR analysis.

Supplementary Figures

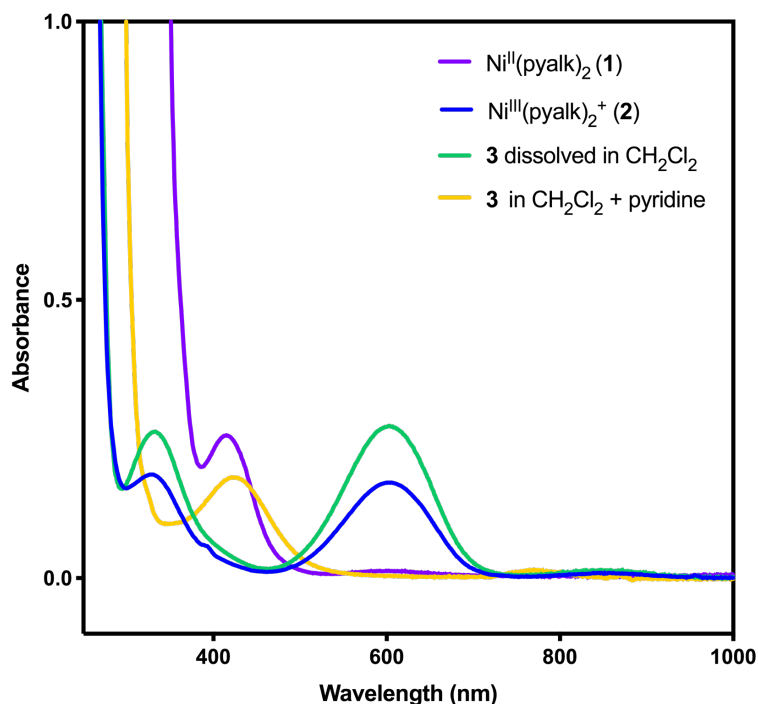


Figure S1. UV-visible spectrum of **3** in the absence (blue) and presence of excess pyridine (yellow). When pure crystals of **3** are dissolved in CH₂Cl₂, the UV-visible spectrum is identical to that of **2**, indicating that the pyridine ligands do not remain bound. When excess pyridine is added to this solution, the UV-visible spectrum of **3** is re-obtained. The spectrum of **1** has been included for comparison.

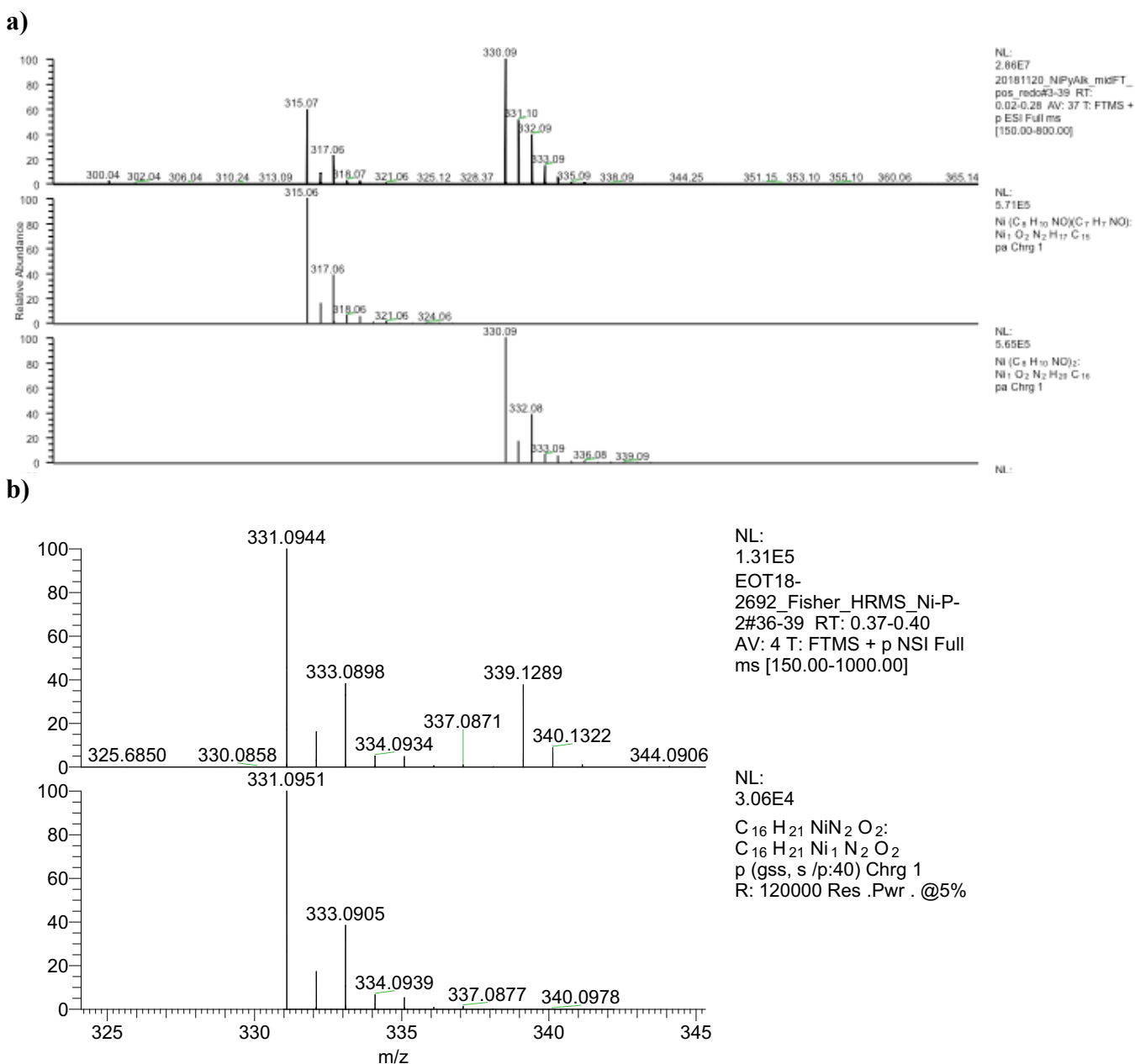


Figure S2. a) Actual (top) and theoretical (middle and bottom) HRMS spectra of $[\text{Ni}(\text{pyalk})_2]^+$ (**2**) in positive mode. b) Actual (top) and theoretical (bottom) HRMS spectrum of $\text{Ni}(\text{pyalk})_2$ (**1**) in positive mode.

a)

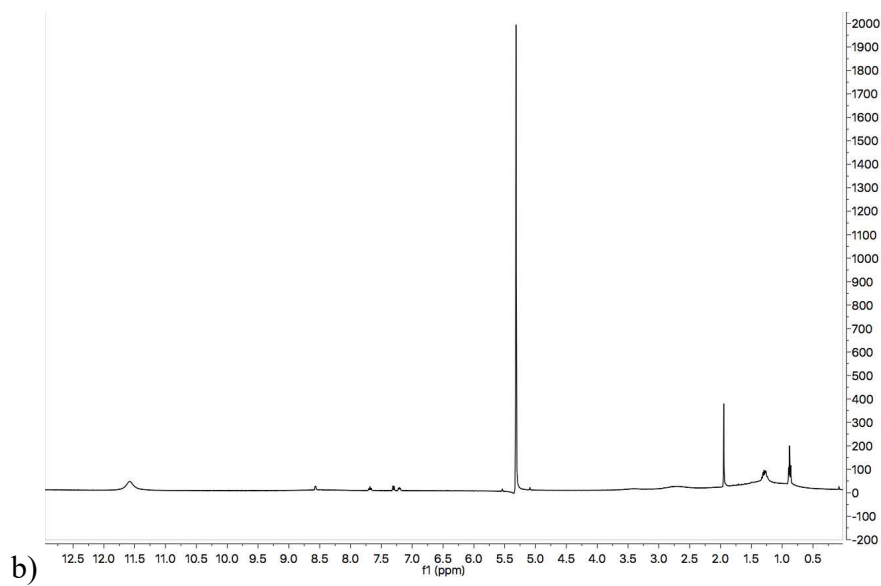
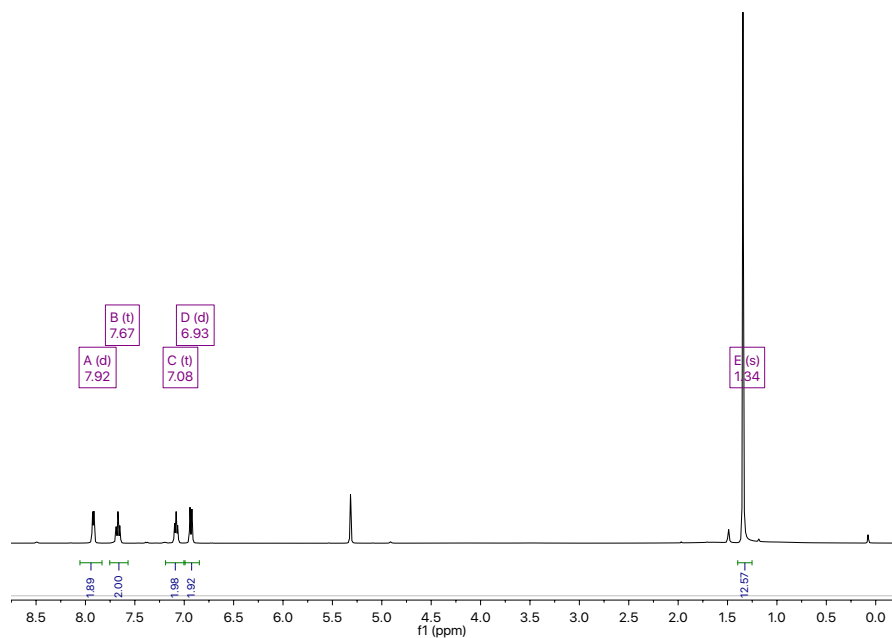


Figure S3. a) ¹H NMR spectrum of a 5 mM solution of Ni(pyalk)₂ (1) in CD₂Cl₂. b) ¹H NMR spectrum of Ni(pyalk)₂⁺ (2) in CD₂Cl₂.

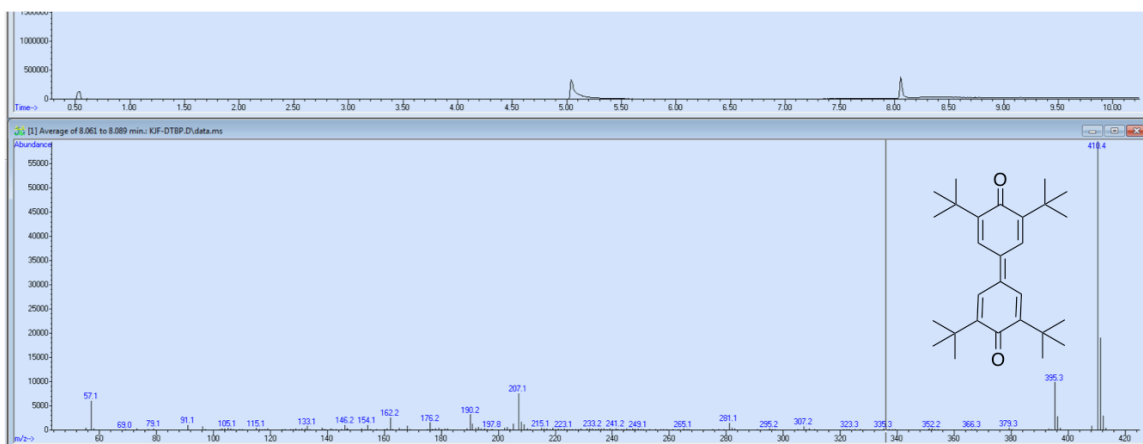


Figure S4. GC-MS spectrum of the products of the reaction between **2** and 2,6-DTBP.

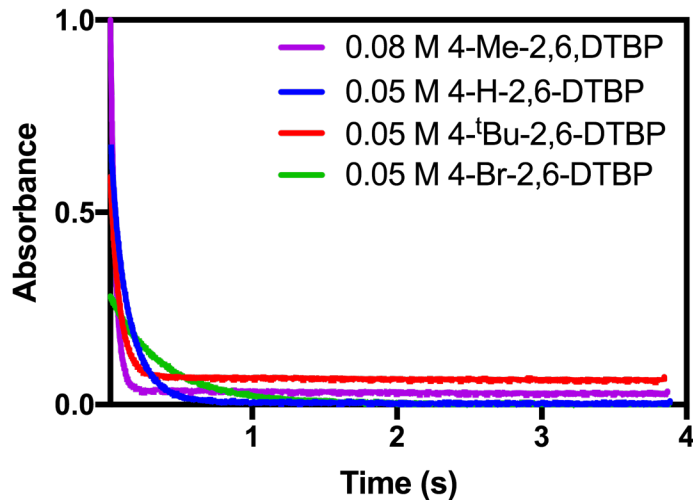


Figure S5. Representative traces of the absorbance at $\lambda = 610$ nm as a function of time for four of the phenol substrates under pseudo-first order conditions.

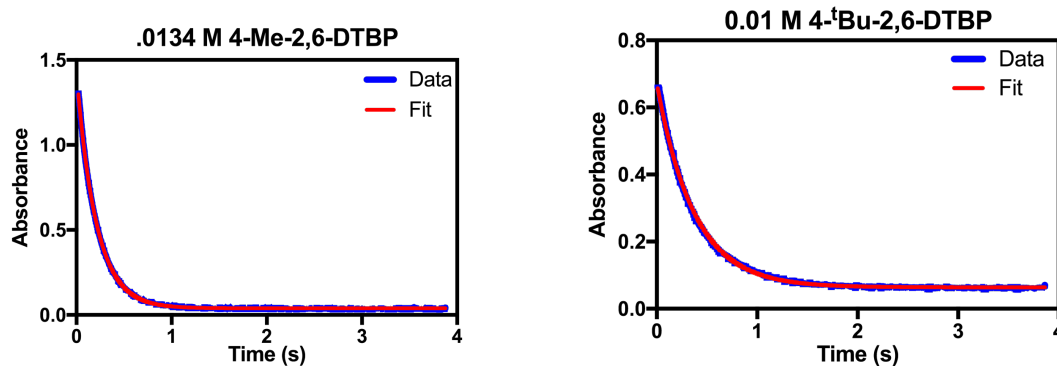


Figure S6. Representative fits of the absorbance at $\lambda = 610$ nm of two of these phenol substrates: 4-Me-2,6-DTBP (left) and 4-^tBu-2,6-DTBP (right).

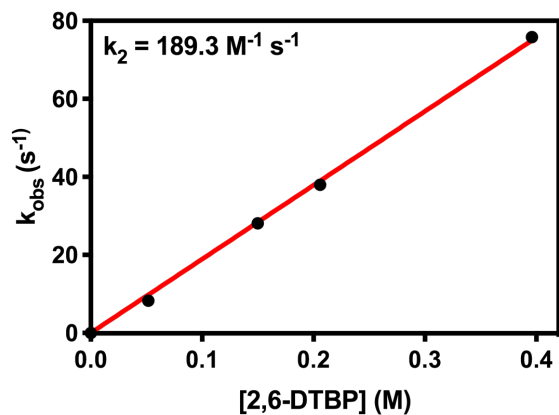


Figure S7. Plot of k_{obs} vs. concentration the pseudo-first order reaction of **2** with 2,6-di-tert-butylphenol in CH_2Cl_2 at 25 °C.

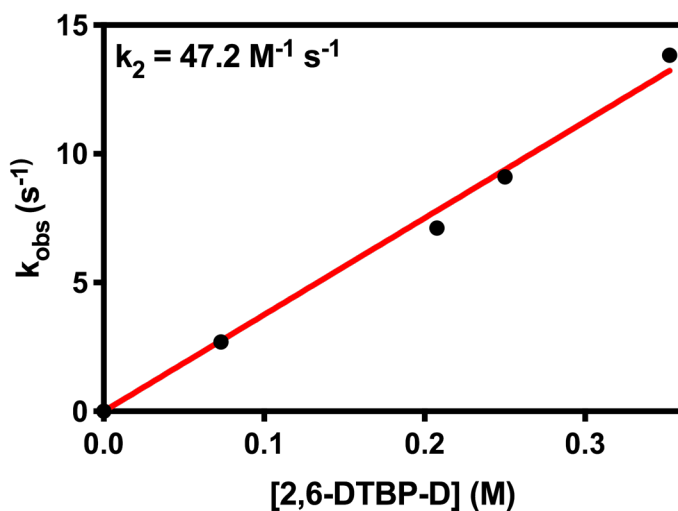


Figure S8. Plot of k_{obs} vs. concentration for the pseudo-first order reaction of **2** with 2,6-di-tert-butylphenol-D in CH_2Cl_2 at 25 °C.

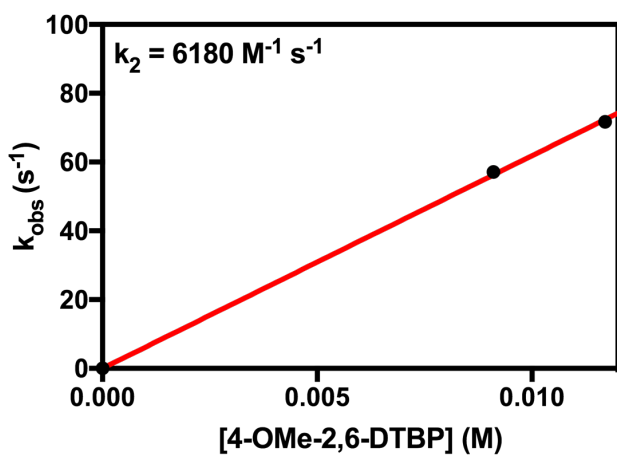


Figure S9. Plot of k_{obs} vs. concentration for the pseudo-first order reaction of **2** with 4-OMe-2,6-di-tert-butyl-phenol in CH_2Cl_2 at 25 °C.

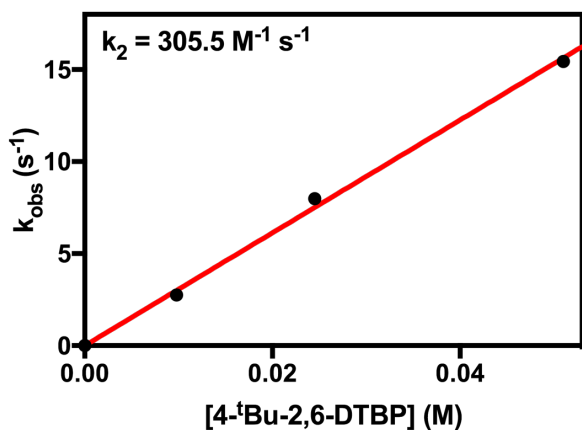


Figure S10. Plot of k_{obs} vs. concentration for the pseudo-first order reaction of **2** with 2,4,6-tri-tert-butylphenol in CH_2Cl_2 at 25 °C.

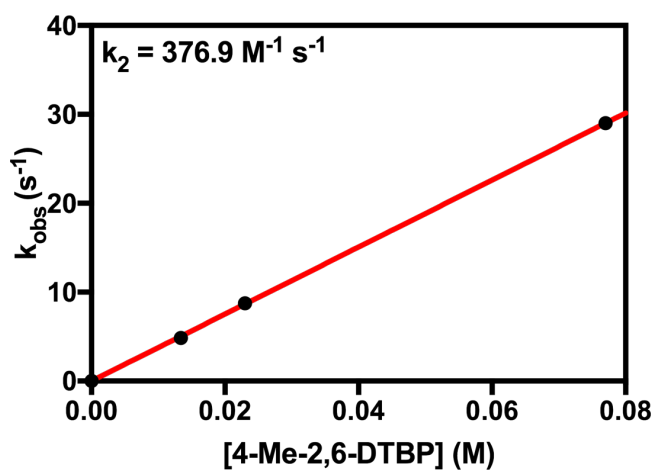


Figure S11. Plot of k_{obs} vs. concentration for the pseudo-first order reaction of **2** with 4-methyl-2,6-di-tert-butylphenol in CH_2Cl_2 at 25 °C.

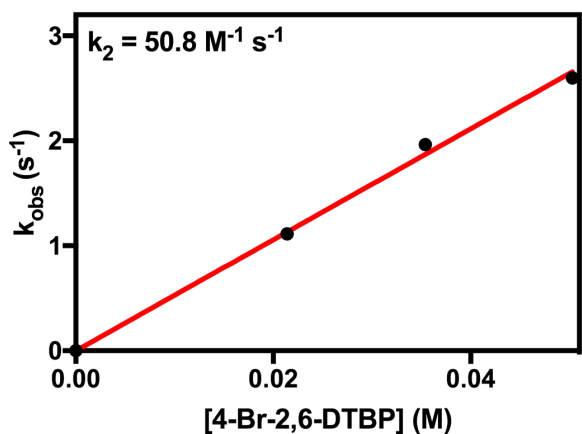


Figure S12. Plot of k_{obs} vs. concentration for the pseudo-first order reaction of **2** with 4-Br-2,6-di-tert-butylphenol in CH_2Cl_2 at 25 °C.

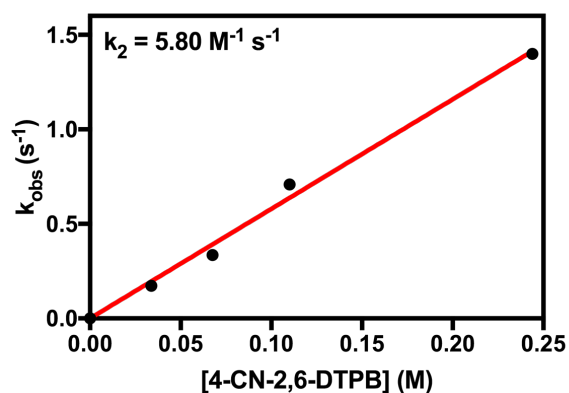


Figure S13. Plot of k_{obs} vs. concentration for the pseudo-first order reaction of **2** with 4-CN-2,6-di-tert-butylphenol in CH_2Cl_2 at 25 °C.

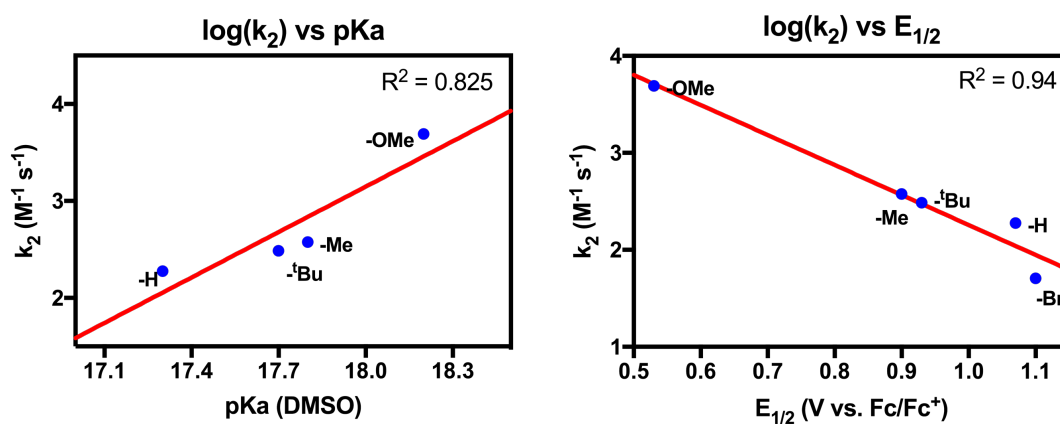


Figure S14. Plots of $\log(k_2)$ vs. substrate pK_a (left) and $\log(k_2)$ vs. substrate redox potential (right). The linear fits of these graphs are poorer than the linear fit of $\log(k_2)$ vs. substrate BDE shown in Figure 5.

Table S1. Summary of kinetic and thermodynamic parameters used for analysis of the reaction of **2** with substituted phenols

-X	$E^{\circ}_{1/2}$ (V vs Fc/Fc ⁺) ^{8,9}	pK _a ^a (DMSO) ¹⁰	BDE (kcal/mol) ^{10,11}	k ₂ (M ⁻¹ s ⁻¹ in CH ₂ Cl ₂)
-OMe	0.53	18.2	78.3	6183
-Me	0.90	17.7	81.0	376.9
- ^t Bu	0.93	17.8	81.2	305.5
-H	1.07	17.3	82.0	189.3
-Br	1.10	-	83.2	50.8
-CN	-	-	84.3	5.80

^a All BDEs reported as measured in DMSO. When multiple BDE values were available, values determined using pK_a and E⁰ data were chosen for the sake of consistency.

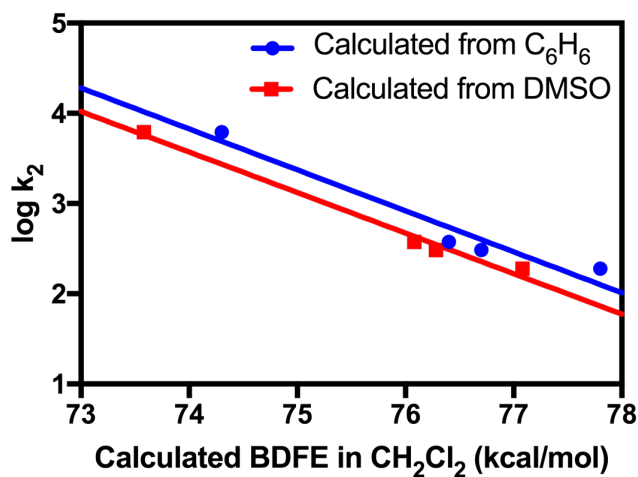


Figure S15. Plot of log(k₂) vs. substrate BDFE in CH₂Cl₂. BDFEs in CH₂Cl₂ were calculated from both BDFEs in DMSO and BDFEs in C₆H₆¹² and were found to be within 0.9 kcal/mol. For a more detailed discussion on calculating BDFEs in CH₂Cl₂, see page S20.

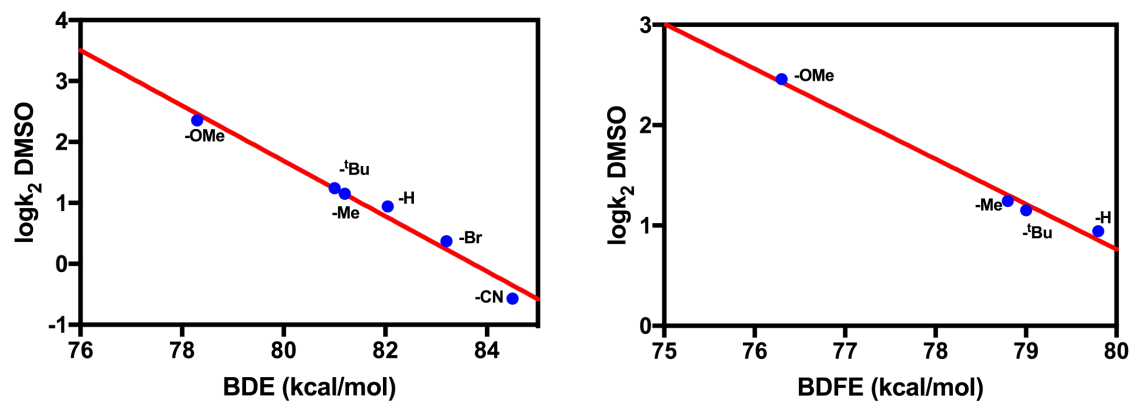


Figure S16. Left: Plot of $\log(k_2)_{\text{DMSO}}$ vs. substrate BDE. Right: Plot of $\log(k_2)_{\text{DMSO}}$ vs. substrate BDFE. BDFE's were calculated from the $\text{p}K_{\text{a}}$ and E^0 data given in equation 2. For a more detailed discussion on calculating $k_{2,\text{DMSO}}$ see page S20.

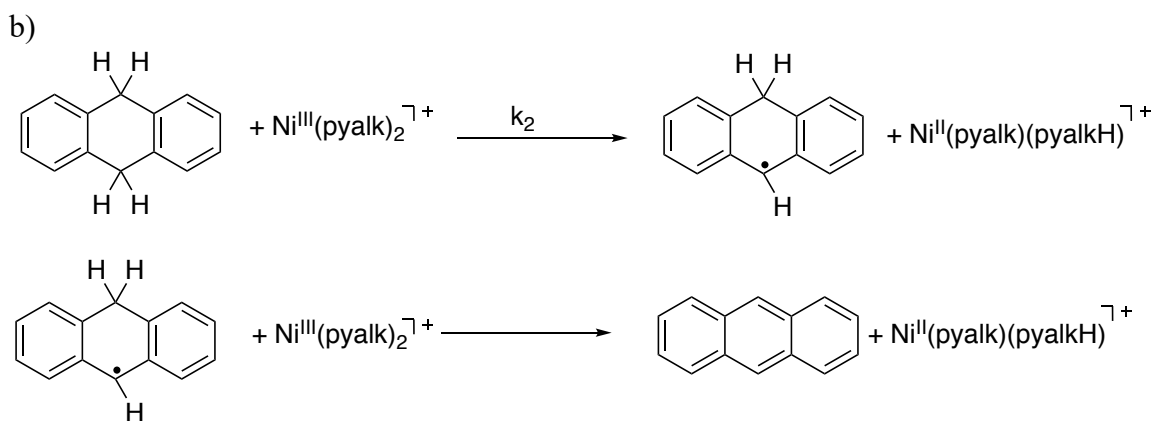
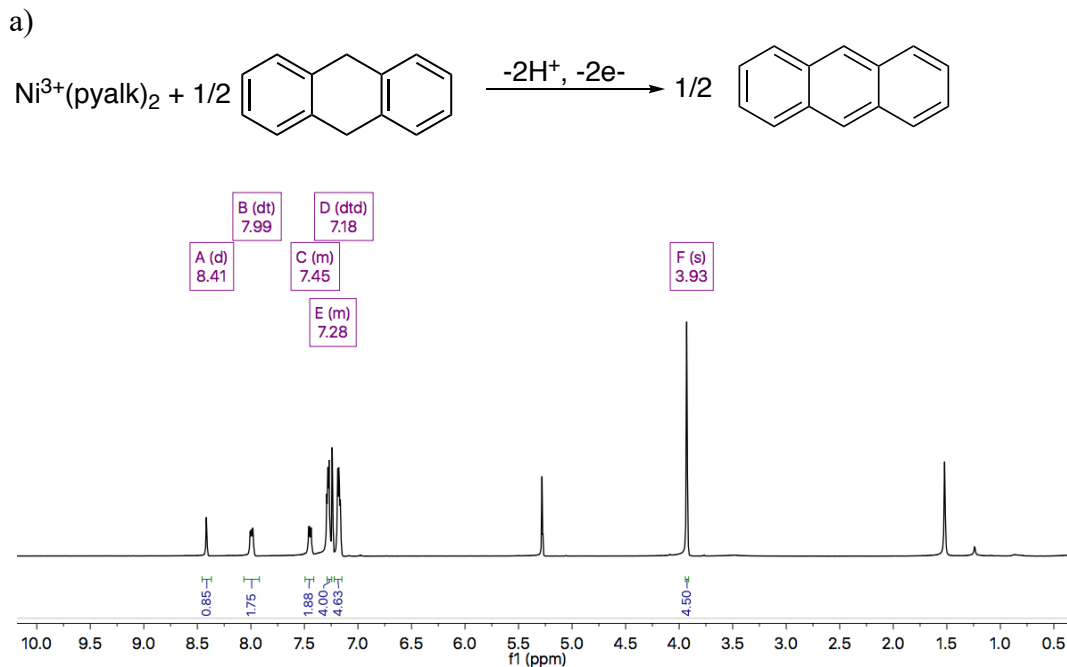


Figure S17. (a) ^1H NMR spectrum of the reaction of a 1 mM solution of dihydroanthracene with a 1 mM solution of **2**. Based on integration, the yield of anthracene is $\sim 50\%$. (b) Proposed mechanism for the $2\text{H}^+/2\text{e}^-$ oxidation of 9,10-dihydroanthracene to anthracene by 2 equivalents of **2**.

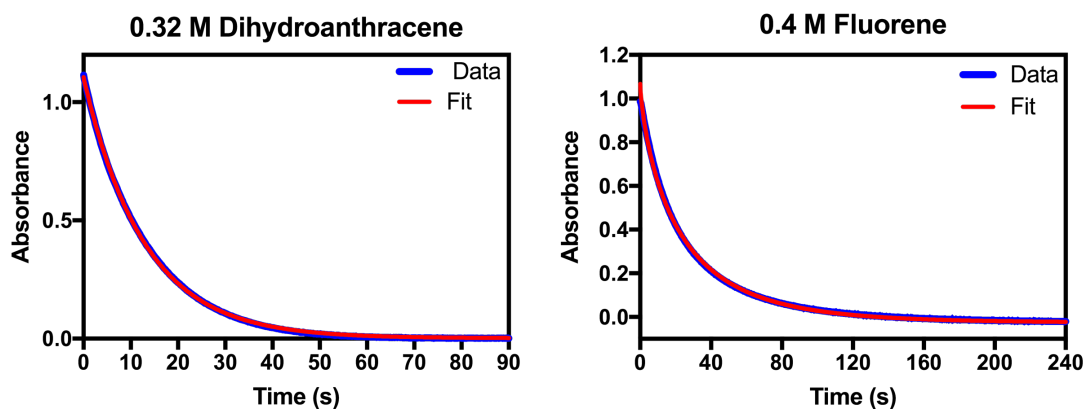


Figure S18. Representative fits of the absorbance at $\lambda = 610$ nm as a function of time for two hydrocarbon substrates: dihydroanthracene (left) and fluorene (right).

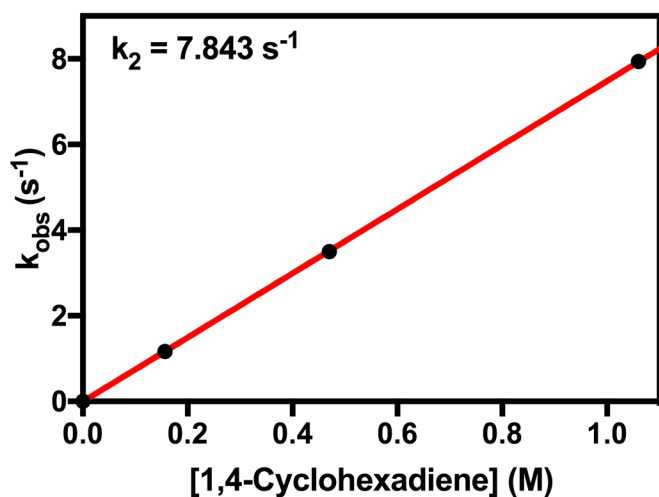


Figure S19. Plot of k_{obs} vs. concentration for the reaction of **2** with 1,4-cyclohexadiene in CH_2Cl_2 at 25 °C.

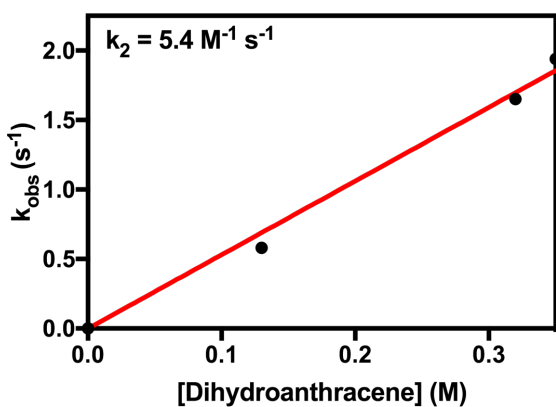


Figure S20. Plot of k_{obs} vs. concentration for the reaction of **2** with dihydroanthracene in CH_2Cl_2 at 25 °C.

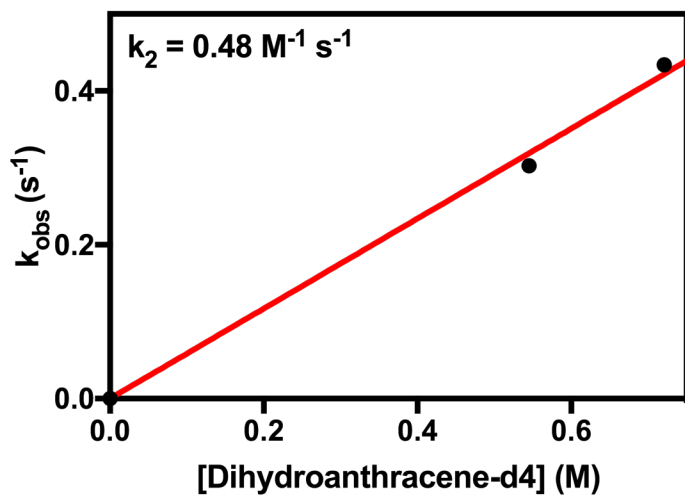


Figure S21. Plot of k_{obs} vs. concentration for the reaction of **2** with dihydroanthracene-d₄ in CH_2Cl_2 at 25 °C.

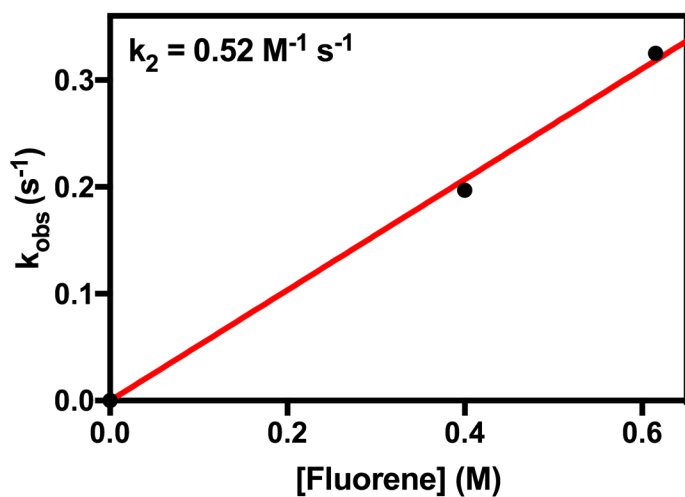


Figure S22. Plot of k_{obs} vs. concentration for the reaction of **2** with fluorene in CH_2Cl_2 at 25 °C.

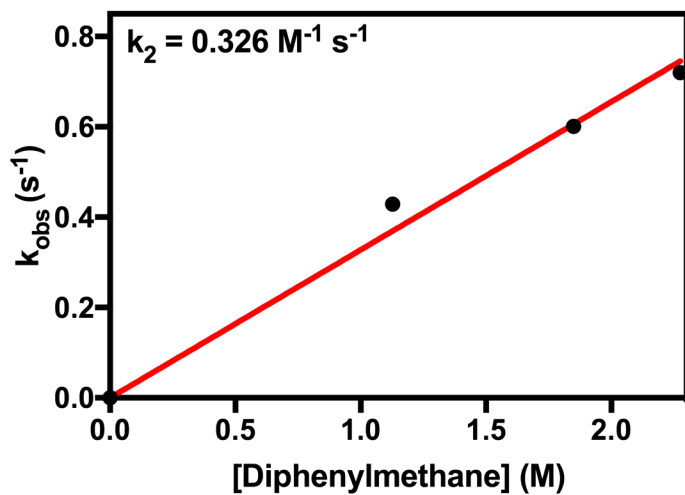


Figure S23. Plot of k_{obs} vs. concentration for the reaction of **2** with diphenylmethane in CH_2Cl_2 at 25 °C.

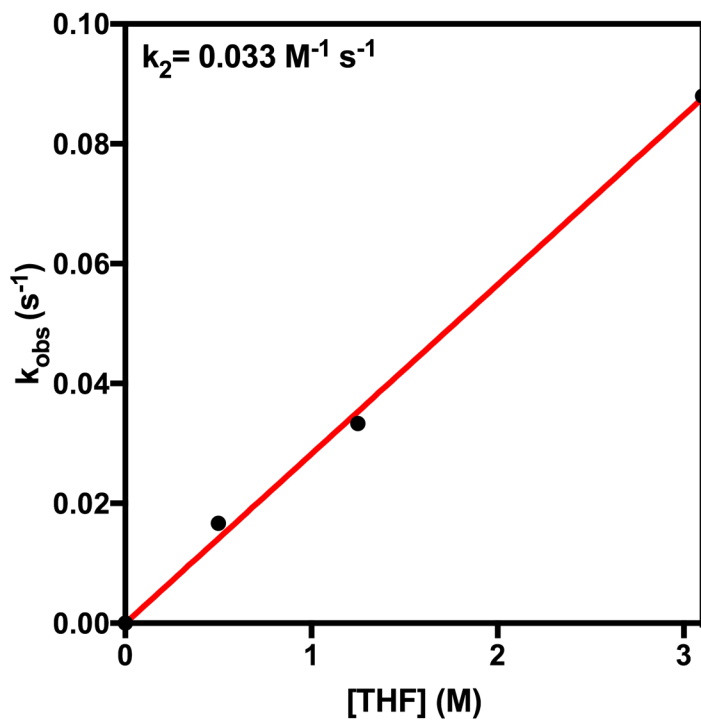


Figure S24. Plot of k_{obs} vs. concentration for the reaction of **2** with tetrahydrofuran (THF) in CH_2Cl_2 at 25 °C.

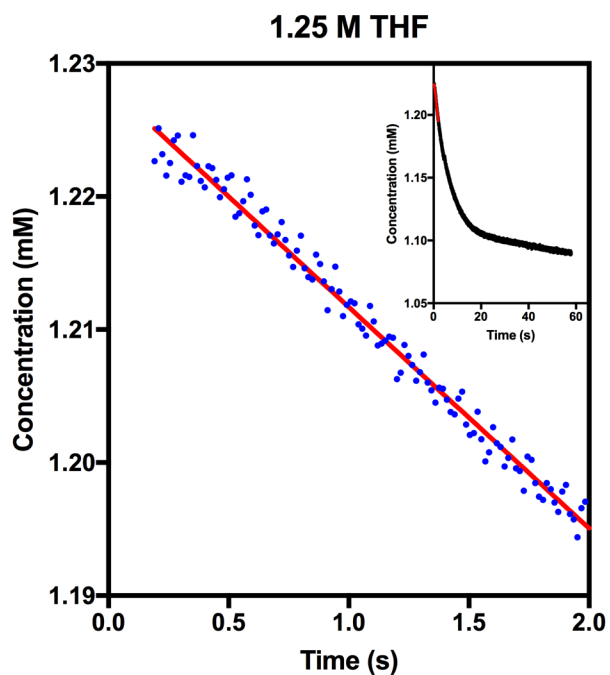


Figure S25. Representative fitting of pseudo-first order reaction between **2** and THF by method of initial rates.

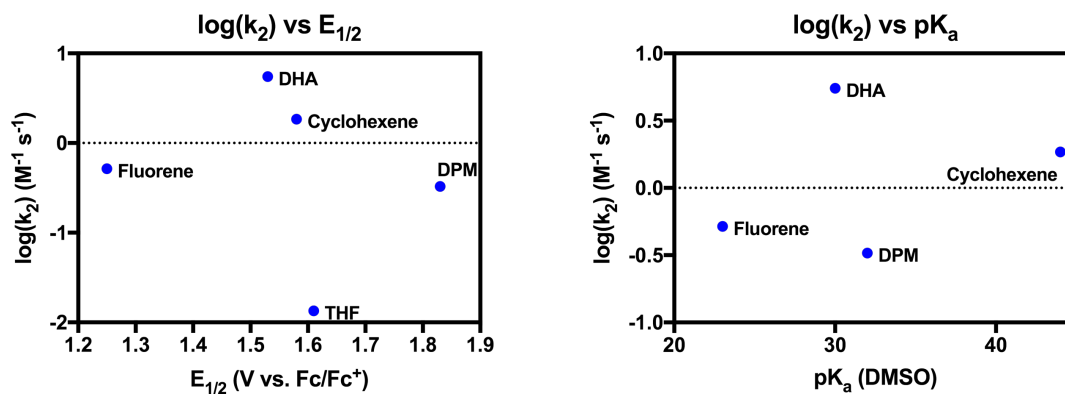


Figure S26. Plots of $\log(k_2)$ vs. substrate redox potential (left) and $\log(k_2)$ vs. substrate pK_a (right). The linear fits of these graphs are poorer than the linear fit of $\log(k_2)$ vs. substrate BDE shown in Figure 7.

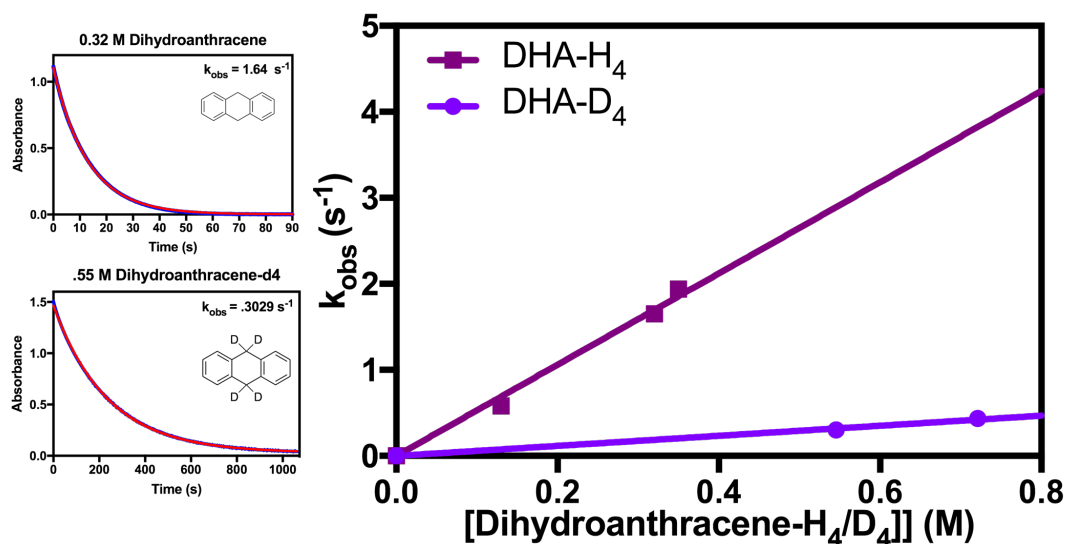


Figure S27. *Left:* representative time trace of the absorbance at $\lambda = 600 \text{ nm}$ for the reaction of **1** with dihydroanthracene (DHA) (top) and DHA-d₄ (bottom). *Right:* Plot of k_{obs} vs. concentration for the reaction of **2** with DHA and DHA-d₄.

Table S2. Summary of thermodynamic and kinetic parameters in our analysis of the reaction of **2** with hydrocarbon substrates.

Substrate	$E^{\circ}_{1/2}$ (V vs Ag/Ag ⁺ in MeCN) ¹³	pK_a (DMSO) ¹⁴	BDE ^a (kcal/mol) ^{12, 15, 16}	k_2 (M ⁻¹ s ⁻¹ in CH ₂ Cl ₂)
1,4-cyclohexadiene	-	-	76 ± 1	7.48
9,10-dihydroanthracene	1.53	30	78 ± 3	5.4
Cyclohexene	1.58	44	81 ± 2	1.94
Fluorene	1.25	23	82 ± 2	0.52
Diphenylmethane	1.83	32	84.3 ± 1	0.33
THF	1.61	-	92 ± 1	0.033

^aAll BDEs reported as measured in DMSO. When multiple BDE values were available, values determined using pK_a and E° data were chosen for the sake of consistency.

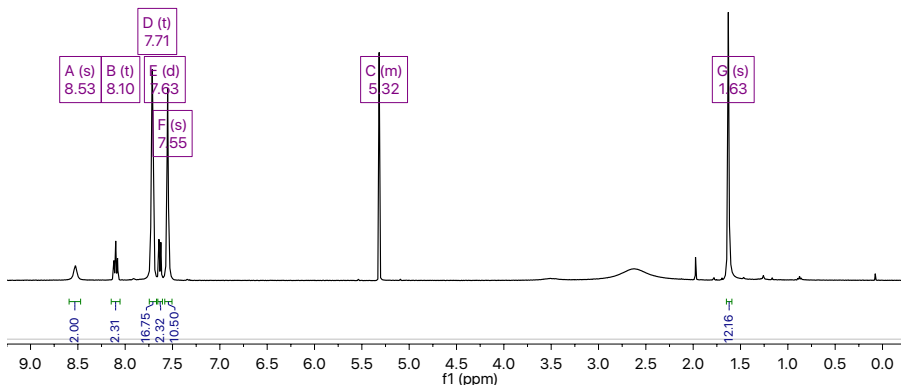


Figure S28. ^1H NMR spectrum of **4**, $[(\text{Ni})(\text{pyalkH})_2][2(\text{BAR}^{\text{F}})]$ in CD_2Cl_2 .

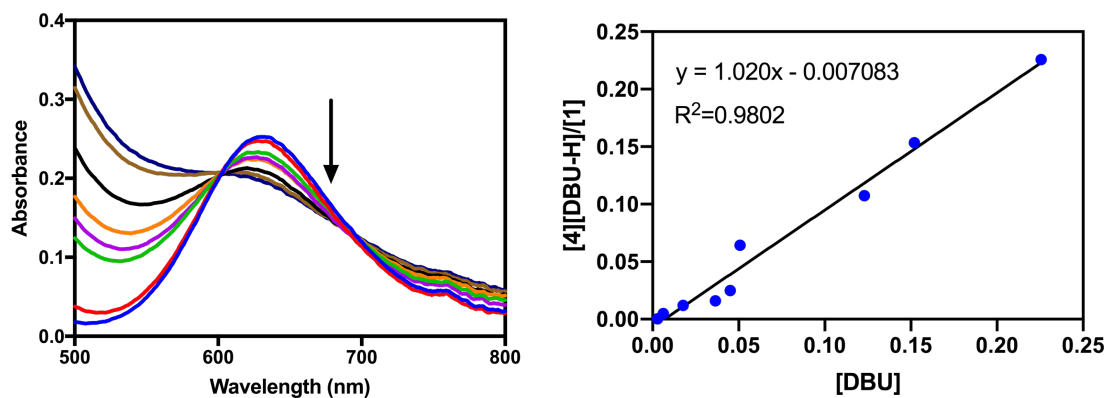


Figure S29. (left) Representative UV-visible spectra of a titration of **4** with DBU. (Right) Linearized titration plot for the conversion of **4** to **1**.

Table S3. Comparison of bond lengths between nickel in various oxidation states and the pyalk oxygen for several compounds discussed in this report.

Compound	Oxidation state of Ni	Ni- O_{pyalk} bond length (\AA)
$\text{Ni}(\text{pyalk})_2$ (1)	2+	1.8365(15)
$[\text{Ni}(\text{pyalk})_2(\text{py})_2]^+$ (3)	3+	1.840(2)
$\text{Ni}(\text{pyalkH})_2(\text{OAc})_2$ (4)	2+	2.076(18)

Discussion of Bond Dissociation Enthalpies/Bond Dissociation Free Energies and Solvent Effects

The interconversion of bond dissociation free energies between solvents for a species XH can be accomplished by converting a BDFE measured in a given solvent to the gas phase and then estimating the free energy of solvation of H• and the difference solvation free energy between X• and XH.^{17, 18}

$$\text{BDFE}_{\text{solv}} = \text{BFDE}_{\text{g}} + \Delta G^{\circ}(\text{H}\bullet) + \Delta G^{\circ}(\text{X}\bullet) - \Delta G^{\circ}(\text{XH})$$

The free energy of solvation of H• is assumed to be the same as the free energy of solvation of H₂ at STP.¹⁷ The difference in free energy of solvation between X• and XH can be estimated as the energy of the XH-solvent hydrogen bond in aprotic solvents. This value can be found using the empirical equation¹⁹:

$$\Delta G^{\circ}_{\text{solv}} = -10.02\alpha_2^H\beta_2^H - 1.492$$

where α_2^H is an hydrogen-bonding acidity parameter unique to each substrate and β_2^H is a hydrogen-bonding basicity parameter unique to each solvent.

This calculation is made for both solvents (in our case, DMSO and CH₂Cl₂), using the parameters found in Table S4, resulting in the following equations:

$$\text{BDFE}_{\text{CH}_2\text{Cl}_2} = \text{BFDE}_{\text{g}} + \Delta G^{\circ}_{\text{solv}}(\text{H}_2)_{\text{CH}_2\text{Cl}_2} - (-10.02\alpha_2^H(0.05) - 1.492)$$

$$\text{BDFE}_{\text{DMSO}} = \text{BFDE}_{\text{g}} + \Delta G^{\circ}_{\text{solv}}(\text{H}_2)_{\text{DMSO}} - (-10.02\alpha_2^H(0.78) - 1.492)$$

These equations are then subtracted from one other and rearranged to provide the following relationship:

$$\text{BDFE}_{\text{CH}_2\text{Cl}_2} = \text{BDFE}_{\text{DMSO}} - [\Delta G^{\circ}_{\text{solv}}(\text{H}_2)_{\text{DMSO}} - (-10.02\alpha_2^H(0.78) - 1.492)] + [\Delta G^{\circ}_{\text{solv}}(\text{H}_2)_{\text{CH}_2\text{Cl}_2} - (-10.02\alpha_2^H(0.05) - 1.492)]$$

For 4-X-2,6-DTBP, $\alpha_2^H = 0.22$ for all 4-X-2,6-DTBP substrates.¹⁷

To ensure that this procedure resulted in reliable BDFE's, the same process was repeated with C₆H₆ instead of DMSO as one of the solvents. The BDFE_{CH₂Cl₂} values found using C₆H₆ BDFE values were within 0.9 kcal/mol of those found using the DMSO values. Plots of log(k₂) vs. BDFE_{CH₂Cl₂} can be found in Figure S15.

Table S4. Solvent parameters used in this analysis.

Solvent	β_2^H ²⁰	$\Delta G^\circ(\text{H}_2)$ ²¹
CH ₂ Cl ₂	0.05	4.5 ¹
DMSO	0.78	5.61
C ₆ H ₆	0.14	4.80

¹Estimated to be the same as $\Delta G^\circ_{\text{solv}}(\text{H}_2)$ in 1,2-dichloroethane as the value in CH₂Cl₂ has not been reported.

The interconversion of k_2 values between different solvents can be found in a similar fashion. The empirical equation relating reaction rates across different solvents can be found in the following equation, where k^{solv} is the rate constant in a hydrogen-bonding solvent and k^0 is the rate constant in a non-hydrogen bonding alkane solvent:¹⁷

$$\log(k^{\text{solv}}) = k^0 - 8.3\alpha_2^H\beta_2^H$$

As above, α_2^H is a hydrogen-bonding acidity parameter unique to each substrate and β_2^H is a hydrogen-bonding basicity parameter unique to each solvent. To convert $k_{2,\text{CH}_2\text{Cl}_2}$ to $k_{2,\text{DMSO}}$, we plugged in the appropriate β_2^H parameters to the equation above to obtain:

$$\log(k^{\text{DMSO}}) = k^0 - 8.3\alpha_2^H(0.78)$$

$$\log(k^{\text{CH}_2\text{Cl}_2}) = k^0 - 8.3\alpha_2^H(0.05)$$

Subtracting these two equations from one another and rearranging provides the following relationship:

$$\log(k^{\text{DMSO}}) = \log(k^{\text{CH}_2\text{Cl}_2}) - 6.06\alpha_2^H$$

$\alpha_2^H = 0.22$ for all 4-X-2,6-DTBP substrates. Plots of $\log(k^{\text{DMSO}})$ vs. BDFE and $\log(k^{\text{DMSO}})$ vs. BDE can be found in Figure S16.

The analyses described above could not be performed for experiments involving the oxidation of hydrocarbons, as α_2^H values are not available for most of those substrates.

Crystallographic Experimental Details:

Low-temperature diffraction data (ω -scans) were collected on a Rigaku R-AXIS RAPID diffractometer coupled to an R-AXIS RAPID imaging plate detector with Mo K α radiation ($\lambda = 0.71073 \text{ \AA}$) for the structure of **1**; similar data were collected on a Rigaku MicroMax-007HF diffractometer coupled to a Saturn994+ CCD detector with Cu K α ($\lambda = 1.54178 \text{ \AA}$) for the structures of **3** and **4**. The diffraction images of **1** were processed and scaled using the Rigaku CrystalClear software (CrystalClear and CrystalStructure; Rigaku/MSK: The Woodlands, TX, 2005). The diffraction images of **3** and **4** were processed and scaled using Rigaku Oxford Diffraction software (CrysAlisPro; Rigaku OD: The Woodlands, TX, 2015). All structures were solved with SHELXT and were refined against F^2 on all data by full-matrix least squares with SHELXL (Sheldrick, G. M. Acta Cryst. 2008, A64, 112–122). All non-hydrogen atoms were refined anisotropically. Unless stated otherwise, hydrogen atoms were included in the model at geometrically calculated positions and refined using a riding model. The isotropic displacement parameters of all hydrogen atoms were fixed to 1.2 times the U value of the atoms to which they are linked (1.5 times for methyl groups). CCDC numbers 1954011 (**1**), 1954012 (**3**), and 1954013 (**5**) contains the supplementary crystallographic data for this paper. These data can be obtained free of charge from The Cambridge Crystallographic Data Center via www.ccdc.cam.ac.uk/data_request/cif.

Crystallographic Information for 1:

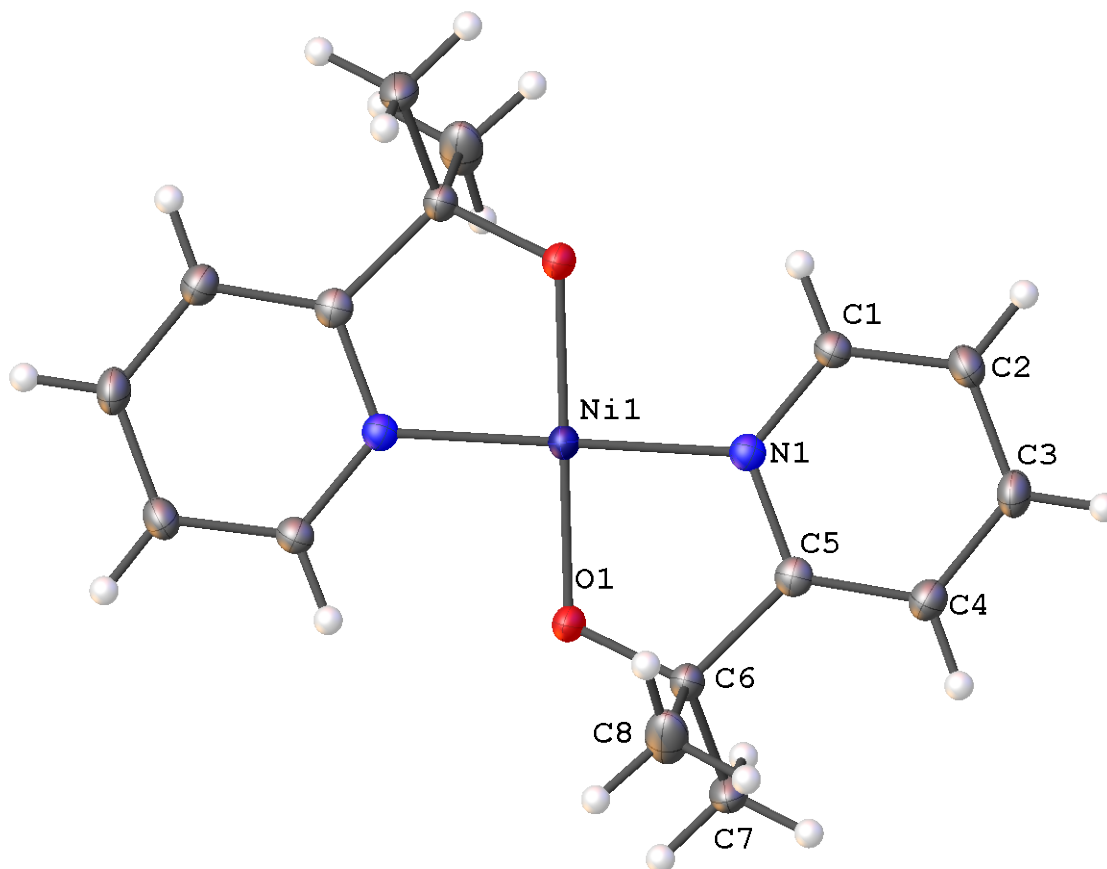


Figure S30. The complete numbering scheme of **1** with 50% thermal ellipsoid probability levels. The hydrogen atoms are shown as circles for clarity.

Table S5. Crystal data and structure refinement for **1**.

Identification code	007a-17123	
Empirical formula	C ₁₆ H ₂₀ N ₂ Ni O ₂	
Formula weight	331.05	
Temperature	93(2) K	
Wavelength	1.54184 Å	
Crystal system	Monoclinic	
Space group	P2 ₁ /n	
Unit cell dimensions	a = 14.557(3) Å	$\alpha = 90^\circ$.
	b = 10.2366(5) Å	$\beta = 141.27(4)^\circ$.
	c = 8.2137(14) Å	$\gamma = 90^\circ$.

Volume	765.8(4) Å ³
Z	2
Density (calculated)	1.436 Mg/m ³
Absorption coefficient	1.871 mm ⁻¹
F(000)	348
Crystal size	0.200 x 0.200 x 0.200 mm ³
Crystal color and habit	Green Plate
Diffractometer	Rigaku Saturn 944+ CCD
Theta range for data collection	5.698 to 66.757°.
Index ranges	-17<=h<=17, -12<=k<=12, -9<=l<=9
Reflections collected	21932
Independent reflections	1361 [R(int) = 0.0690]
Observed reflections (I > 2sigma(I))	1234
Completeness to theta = 66.757°	99.9 %
Absorption correction	Semi-empirical from equivalents
Max. and min. transmission	1.00000 and 0.75022
Solution method	SHELXT-2014/5 (Sheldrick, 2014)
Refinement method	SHELXL-2014/7 (Sheldrick, 2014)
Data / restraints / parameters	1361 / 0 / 99
Goodness-of-fit on F ²	1.048
Final R indices [I>2sigma(I)]	R1 = 0.0281, wR2 = 0.0708
R indices (all data)	R1 = 0.0318, wR2 = 0.0733
Largest diff. peak and hole	0.284 and -0.224 e.Å ⁻³

Crystallographic Information for 3:

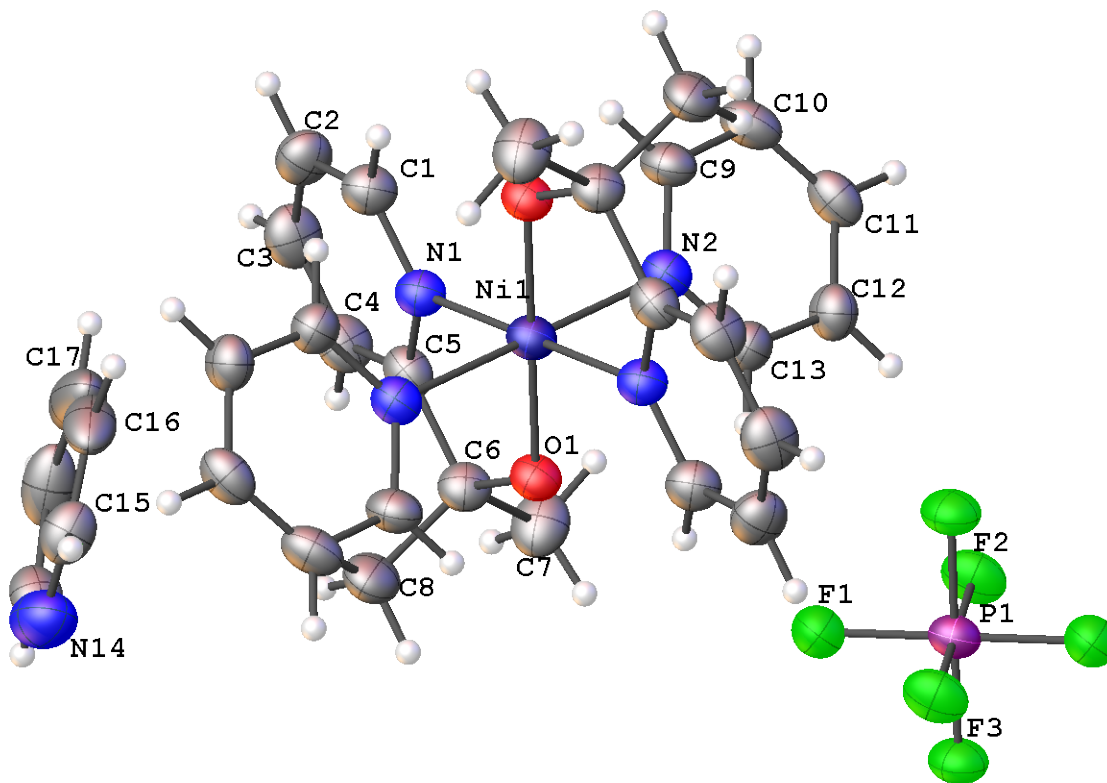


Figure S31. The complete numbering scheme of **3** with 50% thermal ellipsoid probability levels. The hydrogen atoms are shown as circles for clarity. The model is on a crystallographic special position; only the asymmetric unit is labeled.

Table S6. Crystal data and structure refinement for **3**.

Identification code	007a-18050	
Empirical formula	C ₃₁ H ₃₅ F ₆ N ₅ Ni O ₂ P	
Formula weight	713.32	
Temperature	93(2) K	
Wavelength	1.54184 Å	
Crystal system	Monoclinic	
Space group	I2/a	
Unit cell dimensions	a = 22.4997(12) Å	$\alpha = 90^\circ$.
	b = 8.4913(3) Å	$\beta = 111.646(5)^\circ$.
	c = 17.7726(7) Å	$\gamma = 90^\circ$.
Volume	3156.0(3) Å ³	
Z	4	

Density (calculated)	1.501 Mg/m ³
Absorption coefficient	2.017 mm ⁻¹
F(000)	1476
Crystal size	0.100 x 0.100 x 0.050 mm ³
Crystal color and habit	Yellow Plate
Diffractometer	Rigaku Saturn 944+ CCD
Theta range for data collection	4.228 to 66.893°.
Index ranges	-26<=h<=26, -9<=k<=9, -21<=l<=21
Reflections collected	54705
Independent reflections	2801 [R(int) = 0.0908]
Observed reflections (I > 2sigma(I))	2231
Completeness to theta = 66.893°	99.4 %
Absorption correction	Semi-empirical from equivalents
Max. and min. transmission	1.00000 and 0.71733
Solution method	SHELXT-2014/5 (Sheldrick, 2014)
Refinement method	SHELXL-2014/7 (Sheldrick, 2014)
Data / restraints / parameters	2801 / 0 / 214
Goodness-of-fit on F ²	1.071
Final R indices [I>2sigma(I)]	R1 = 0.0526, wR2 = 0.1320
R indices (all data)	R1 = 0.0692, wR2 = 0.1434
Largest diff. peak and hole	0.487 and -0.512 e.Å ⁻³

Crystallographic information for 5:

The proton on O1 was found in the difference map and freely refined.

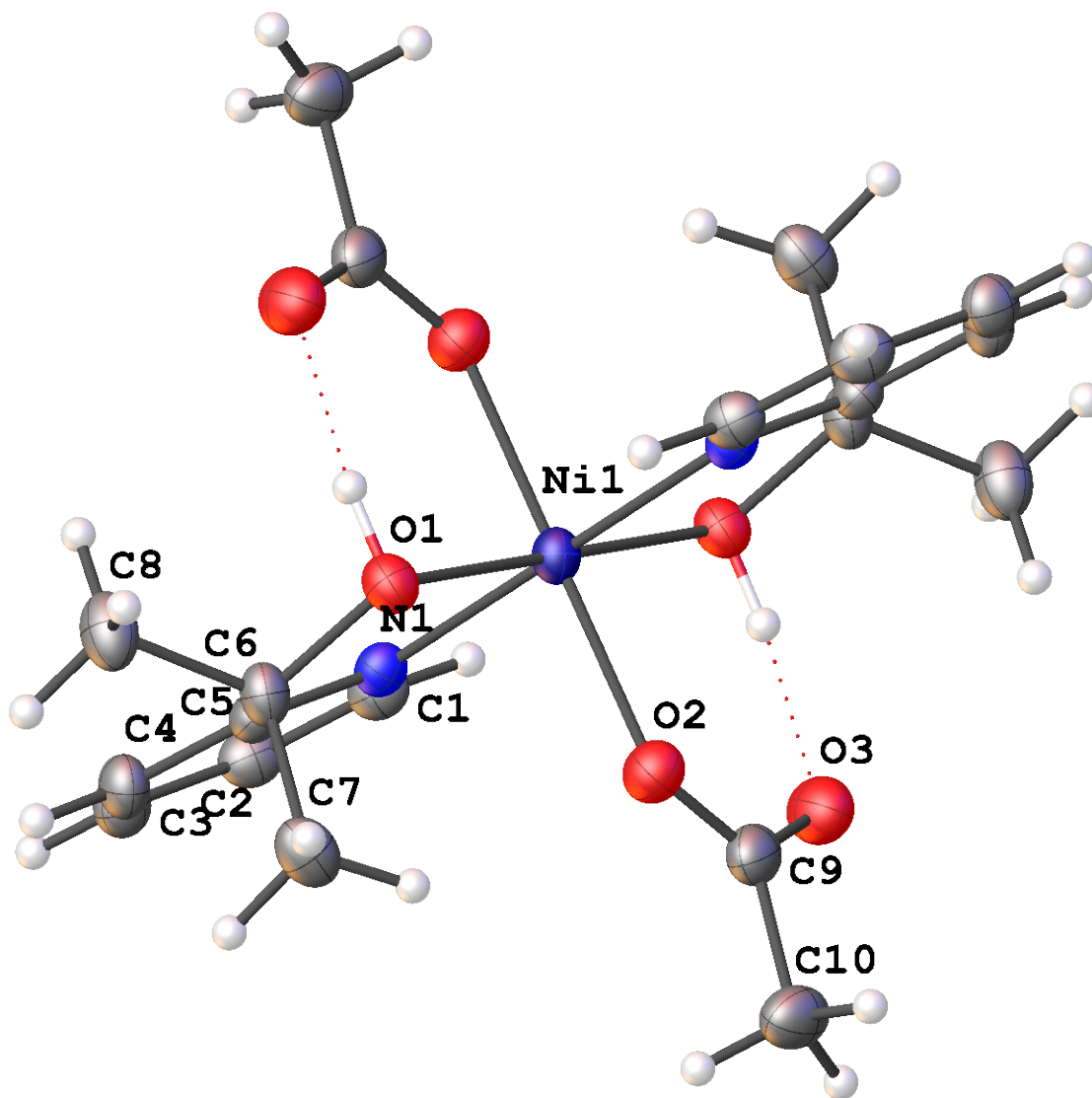


Figure S32. The complete numbering scheme of **5** with 50% thermal ellipsoid probability levels. The hydrogen atoms are shown as circles for clarity. The model is on a crystallographic special position; only the asymmetric unit is labeled.

Table S7. Crystal data and structure refinement for **5**.

Identification code	spider-16039
Empirical formula	C ₂₀ H ₂₈ N ₂ Ni O ₆
Formula weight	451.15
Temperature	93(2) K
Wavelength	0.71075 Å

Crystal system	Monoclinic	
Space group	P2 ₁ /n	
Unit cell dimensions	a = 8.3939(4) Å	α = 90°.
	b = 14.9329(8) Å	β = 108.791(8)°.
	c = 8.7611(6) Å	γ = 90°.
Volume	1039.63(11) Å ³	
Z	2	
Density (calculated)	1.441 Mg/m ³	
Absorption coefficient	0.972 mm ⁻¹	
F(000)	476	
Crystal size	0.200 x 0.200 x 0.050 mm ³	
Crystal color and habit	green plate	
Diffractometer		
Theta range for data collection	3.226 to 25.008°.	
Index ranges	-9 ≤ h ≤ 9, -17 ≤ k ≤ 17, -10 ≤ l ≤ 10	
Reflections collected	20757	
Independent reflections	1829 [R(int) = 0.0888]	
Observed reflections (I > 2σ(I))	1536	
Completeness to theta = 25.008°	99.8 %	
Absorption correction	Semi-empirical from equivalents	
Max. and min. transmission	1.000 and 0.778	
Solution method	?	
Refinement method	SHELXL-2014/7 (Sheldrick, 2014)	
Data / restraints / parameters	1829 / 0 / 140	
Goodness-of-fit on F ²	1.046	
Final R indices [I > 2σ(I)]	R1 = 0.0418, wR2 = 0.0800	
R indices (all data)	R1 = 0.0538, wR2 = 0.0846	
Largest diff. peak and hole	0.303 and -0.335 e.Å ⁻³	

References

1. Y.-L. Wong, Q. Yang, Z.-Y. Zhou, H. K. Lee, T. C. W. Mak and D. K. P. Ng, *New J. Chem.*, 2001, **25**, 353-357.
2. T. Kurahashi, A. Kikuchi, Y. Shiro, M. Hada and H. Fujii, *Inorg. Chem.*, 2010, **49**, 6664-6672.
3. C. R. Goldsmith, R. T. Jonas and T. D. P. Stack, *J. Am. Chem. Soc.*, 2002, **124**, 83-96.
4. D. F. Evans and D. A. Jakubovic, *J. Chem. Soc., Dalton Trans.*, 1988, 2927-2933.
5. S. Stoll and A. Schweiger, *J. Magn. Reson.*, 2006, **178**, 42-55.
6. C. T. Saouma, W. Kaminsky and J. M. Mayer, *J. Am. Chem. Soc.*, 2012, **134**, 7293-7296.
7. V. W. Manner, T. F. Markle, J. H. Freudenthal, J. P. Roth and J. M. Mayer, *Chem. Commun.*, 2008, 256-258.
8. J. Y. Lee, R. L. Peterson, K. Ohkubo, I. Garcia-Bosch, R. A. Himes, J. Woertink, C. D. Moore, E. I. Solomon, S. Fukuzumi and K. D. Karlin, *J. Am. Chem. Soc.*, 2014, **136**, 9925-9937.
9. S. Kundu, E. Miceli, E. R. Farquhar and K. Ray, *Dalton Trans.*, 2014, **43**, 4264-4267.
10. F. G. Bordwell and X.-M. Zhang, *J. Phys. Org. Chem.*, 1995, **8**, 529-535.
11. S. Kundu, P. Chernev, X. Engelmann, C. S. Chung, H. Dau, E. Bill, J. England, W. Nam and K. Ray, *Dalton Trans.*, 2016, **45**, 14538-14543.
12. J. J. Warren, T. A. Tronic and J. M. Mayer, *Chem. Rev.*, 2010, **110**, 6961-7001.
13. Z. Blum, L. Cedheim and L. Ebersson, *Acta Chem. Scand.*, 1977, **31b**, 662-666.
14. F. G. Bordwell, *Acc. Chem. Res.*, 1988, **21**, 456-463.
15. J. R. Bryant and J. M. Mayer, *J. Am. Chem. Soc.*, 2003, **125**, 10351-10361.
16. L. J. J. Laarhoven and P. Mulder, *J. Phys. Chem. B*, 1997, **101**, 73-77.
17. J. J. Warren and J. M. Mayer, *Proc. Natl. Acad. Sci. U. S. A.*, 2010, **107**, 5282.
18. T. R. Porter and J. M. Mayer, *Chem. Sci.*, 2014, **5**, 372-380.
19. M. H. Abraham, P. L. Grellier, D. V. Prior, R. W. Taft, J. J. Morris, P. J. Taylor, C. Laurence, M. Berthelot, R. M. Doherty and et al., *J. Am. Chem. Soc.*, 1988, **110**, 8534-8536.
20. M. H. Abraham, P. L. Grellier, D. V. Prior, J. J. Morris and P. J. Taylor, *J. Chem. Soc. Perk. Trans. 2*, 1990, 521-529.
21. *Solubility Data Series: Hydrogen and Deuterium*, Pergamon Press Inc, Elmsford, New York, 1981.